ADVANCED FUNCTIONAL MATERIALS
www.afm-journal.de

A Novel Bioinspired Switchable Adhesive with Three Distinct Adhesive States

*Paula Yagüe Isla and Elmar Kroner**

A novel switchable adhesive, inspired by the gecko's fibrillar dry attachment system, is introduced. It consists of a patterned surface with an array of mushroom-shaped pillars having two distinct heights. The different pillar heights allow control of the pull-off force in two steps by application of a low and a high preload. For low preload, only the long pillars form contact, resulting in a low pull-off force. At higher preload, all pillars form contact, resulting in high pull-off force. Even further loading leads to buckling induced detachment of the pillars which corresponds to extremely low pull-off force. To achieve the respective samples a new fabrication method called double inking is developed, to achieve multiple-height pillar structures. The adhesion performance of the two-step switchable adhesive is analysed at varying preload and for different pillar aspect ratios and height relations. Finally, the deformation behavior of the samples is investigated by in situ monitoring.

1. Introduction

Bioinspired adhesives, as, for example, found on gecko toes, have fascinated mankind since a long time.[1] Especially during recent years there have been notable breakthroughs in understanding the mechanisms of bioinspired adhesives and mimicking such biological dry adhesion systems.[2,3] The reason for the large attention of the so-called "gecko effect" is due to the unique combination of adhesive properties: high adhesion, easy detachment, reversibility, and cleanliness. The dry adhesion system of geckos is based on a complex hierarchical structure of long tilted keratinous stems, which branch into very fine anisotropic contacts.[4] This complex geometry allows the gecko to form a large contact area even with rough surfaces, thus enhancing the adhesive interaction. Especially the anisotropy of the structures in combination with the biomechanics of their locomotion is responsible for the switchability of the adhesion system,[5] namely quick attachment and detachment, which is one of the key properties of bioinspired dry adhesives.

P. Y. Isla, Dr. E. Kroner
INM – Leibniz Institute for New Materials
Campus D2 2, 66123 Saarbrücken, Germany
E-mail: elmar.kroner@inm-gmbh.de
P. Y. Isla
Saarland University
Campus D2 2, 66123 Saarbrücken, Germany

DOI: 10.1002/adfm.201500241

Numerous approaches to mimic gecko-inspired adhesives have recently been published.[3,5,6] Lately, the focus was set to fabrication of switchable bioinspired adhesives. For example, Northen et al. succeeded in developing a composite consisting of an adhesive polymer and magnetic nickel cantilevers.[7] By means of a magnetic field they were able to change the orientation of the cantilevers and thus the adhesive performance. Paretkar et al. showed that adhesion of elastomeric pillars can be switched off by mechanical overloading which causes reversible buckling of the structures.[8] Del Campo and co-workers have used a liquid crystal elastomer which allowed to approach and retract an array of pillars, either allowing or preventing them to form adhesive contact.[9] By applying a low-voltage pulse, Vogel and Steen succeeded in controlling the surface tension force within liquid bridges to generate switchable adhesion.[10] Nadermann et al. used a metastable, film-terminated, structure which allowed them to switch between a collapsed and an uncollapsed state using air pressure.[11] The approach to pattern a wrinkled surface by Jeong et al. led to an adhesive which was switchable upon stretching due to a change in orientation of the adhesive structure along the surface caused by the change in waviness of the wrinkles.[12] Shape memory polymers allow a specific change of their material properties by an external stimulus such as light or temperature. Reddy et al. used a shape memory polymer where the fibrils were mechanically bent and recovered by increasing temperature,[13] thus changing the adhesive performance.

Despite these promising approaches, there is still a challenge to improve the controllability and reversibility of switchable adhesion. In the present study, we investigated a novel aspect of switchability in bioinspired adhesives, namely to achieve a switchable adhesive with more than two adhesive states. While current bioinspired switchable adhesives usually have a high and a low adhesion state, we have designed a switchable adhesive, which allows switching mechanically between "low," "high," and "very low" adhesive state. This multistep switchable adhesion is achieved by macrofibrils with defined tip geometry and two distinct lengths. Depending on the applied compressive load, the number of contacting fibrils can be controlled. This concept may lead to the development of adhesion systems which allow precise control of the pull-off force as a function of preload.

2. Results

Samples with different hexagonally ordered arrays of pillars were successfully prepared. **Figure 1** shows a representative sample

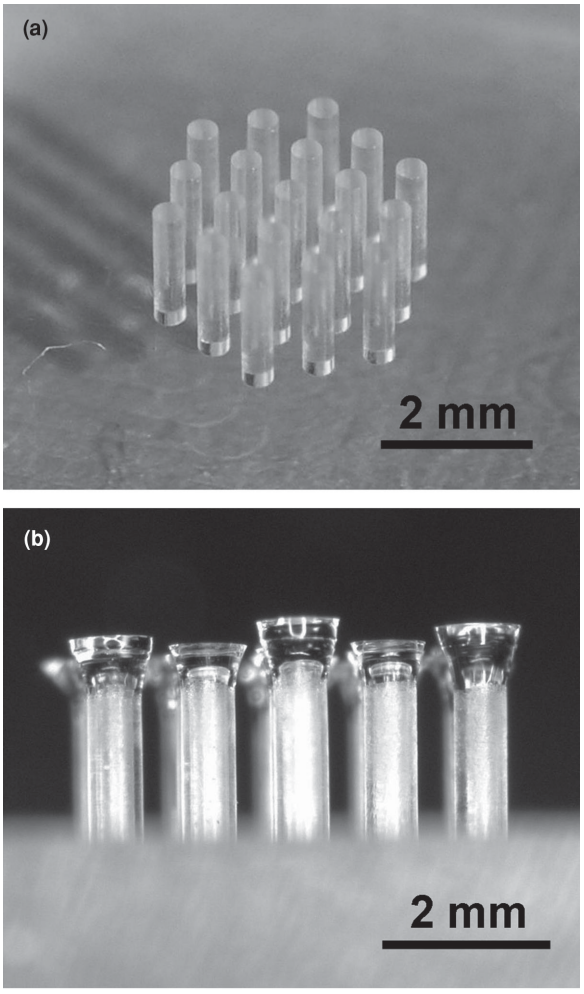

Figure 1. PDMS sample before the dipping process a) and after the dipping process showing pillars with two different lengths b). Note that the artifacts in the pillar tips in (b) are due to reflections at the curved surface.

obtained after molding (Figure 1a) and after the full dipping process (Figure 1b). The different lengths caused by the double dipping procedure are clearly visible in Figure 1b. In the following, LP indicates the long pillars, while SP stands for short pillars.

The heights of the pillars as well as their diameters were determined using an optical microscope (Keyence VHX-2000D equipped with a VH-Z20R/W lens). **Table 1** summarizes the measured geometric parameters.

Adhesion tests were performed on all PDMS samples with the custom-made macroscopic adhesion measurement device (MAD) adhesion tester. **Figure** 2a shows force–displacement curves for three exemplary adhesion measurements with low, medium, and high preload. The sample was approached towards the probe until it formed contact. Then, the sample was loaded until a certain displacement was reached. The maximum applied compressive load is defined as preload. The probe was then retracted again and pulled off the sample. The maximum applied force is defined as pull-off force. Figure 2b shows the tensile part of Figure 2a in larger magnification.

The dotted line represents a measurement performed with low preload. The graph shows features which are typical for patterned surfaces, namely there is a single slope in the

Table 1. Summary of the geometric parameters of the different samples.

	SP height [µm]	LP height [µm]	Δ Height [%]	SP tip Ø [µm]	LP tip Ø [µm]	Δ Tip Ø [%]
AR 4.0	1590	1700	6.9	570	630	10.5
AR 4.5	1800	1880	4.4	620	680	9.7
AR 5.0	1980	2100	6.1	640	680	6.3

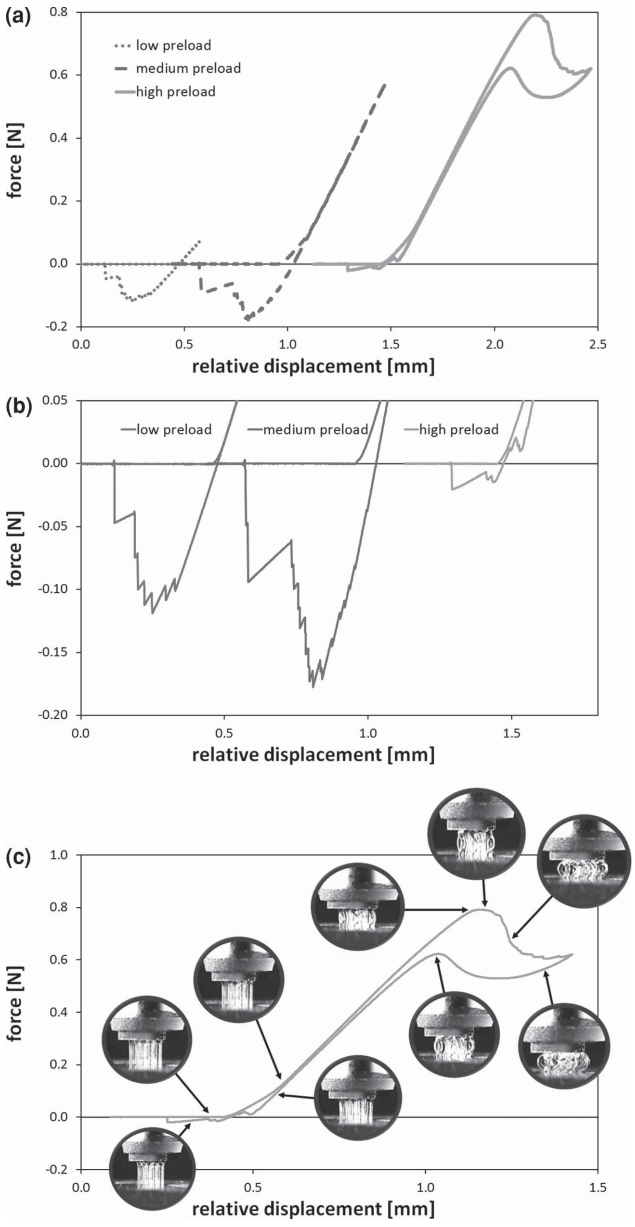

Figure 2. The graphs show force-displacement curves obtained from experiments with low, intermediate, and high preload. a) Stepwise detachment of LP for low preload, SP and LP for intermediate preload, and a hysteresis in the compressive part and low detachment forces at high preload are found. b) The tensile part of (a) is magnified. c) The adhesion curve at high preload and the corresponding in situ pictures.

compressive, and a saw-tooth like detachment in the tensile, part of the force–distance curve. In situ observations allow correlation of each pull-off peak to the detachment of individual pillars, in this case seven detachment peaks which correspond to the seven LP. The applied preload was too low for the SP to form contact with the probe.

For the dashed curve, where a medium preload is targeted, the sample forms contact with the LP and initially has the same slope as for the low preload adhesion test. Then, the slope of the force–displacement curve suddenly increases at a certain load, in this case for a preload of ≈0.08 N. In situ monitoring shows that the SP form contact at this point. The sample is further loaded and the probe is then retracted again. In the tensile part of the sample a considerably higher pull-off force is measured and 19 pull-off peaks can be identified, each corresponding to the detachment of an individual pillar. In situ visualization shows that the first peaks correspond to the detachment of the SP of the array, while the final detachment peaks are due to detachment of the longer pillars.

The third exemplary curve (solid line) with a high target preload shows considerably different features. At low preload the graph follows the same trend as found for medium pull-off force, namely initially having a low slope and, after the SP come into contact, showing a higher slope. Then, at a certain critical load (here ≈0.8 N), a maximum preload is reached. Further displacement leads to a drop in load, which corresponds to an observed buckling of the pillars. During unloading, the graph follows a different path, opening up a hysteresis, where the pillars visually unbuckle. When the sample is finally unloaded and a tensile force is applied, detachment occurs immediately, in some cases even in the compressive part of the curve. The number of detachment peaks is much lower and the peaks seem to be smeared out. The resulting pull-off force is very low. Figure 2c shows the adhesion experiment at high preload as described above with the corresponding in situ pictures of the sample.

The adhesive response of the samples can thus be grouped in three preload phases: i) at low preload only LP form contact with the probe resulting in and a low pull-off force, ii) at intermediate preload both LP and SP form contact with the probe and a high pull-off force occurs, and iii) at high preload, the pillars buckle and the pull-off force breaks down.

Figure 3 summarizes all adhesion experiments for the three different ARs AR 4.0, AR 4.5, and AR 5.0, tested with a velocity of 20 and 60 μm s^{-1}. Graphs showing the pull-off force as a function of preload are given in Supplementary Information. The following observations can be made.

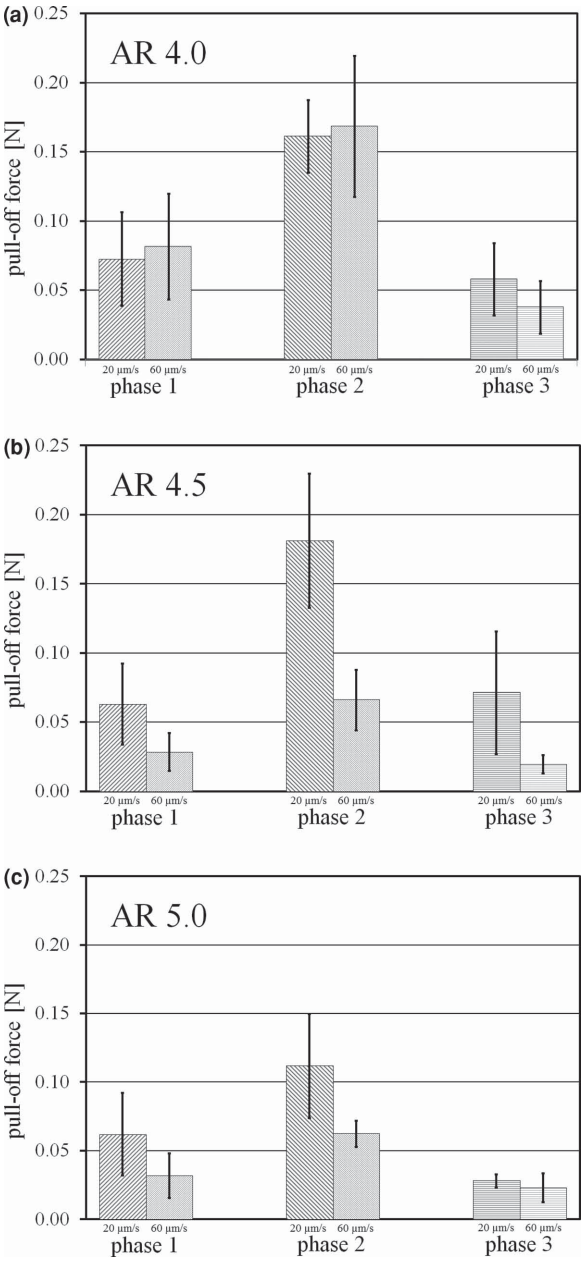

Figure 3. Pull-off forces measured on samples with different AR at different velocities. The results stem from a) AR 4.0, b) AR 4.5, and c) AR 5.0 samples.

i. For each tested AR and velocity the three previously described phases can be detected, namely "phase 1" where low preload leads to low pull-off forces, "phase 2" where intermediate preload leads to high pull-off forces, and "phase 3," where high preload leads to very low pull-off forces. Although there are some cases where the phase 1 pull-off force is similar to the phase 3 pull-off force, the general trend remains.
ii. With increasing testing velocity, the pull-off force decreases. The pull-off force for AR 4.0 samples are similar for the two testing velocities of 20 and 60 μm s^{-1}, but a considerable difference of at least a factor 2 was found for the AR 4.5 and AR 5.0 samples.
iii. With increasing AR, the pull-off force decreases. The pull-off forces are found for the AR 4.0 samples. While the 20 μm s^{-1} experiments for the AR 4.5 samples show similar results to the AR 4.0 samples, the 60 μm s^{-1} experiments already exhibit a notable decrease in pull-off force. For the AR 5.0 samples, the pull-off forces for both testing velocities are considerably lower compared to the AR 4.0 samples.
iv. Although the individual experiments show an extremely low scatter below ±3%, the overall scatter is relatively large. This becomes obvious in the specific experiments, which are shown in the Supporting Information.

In the following section we will discuss these findings and compare the results to adhesive systems and effects published in previous papers.

3. Discussion

Earlier publications have reported on various different ways to fabricate mushroom shaped tips. With our new method we succeeded in both increasing the diameter of selected mushroom pillar tips and, at the same time, increasing the pillar length. The resulting samples were tested for their adhesive properties and exhibited the expected three different adhesive states.

3.1. Low Preload

The longest pillars make contact with the probe, causing a medium pull-off force. The seven LP were identified to first form contact with the probe directly by in situ observation and indirectly by receiving seven distinct detachment peaks during pull-off, where each peak corresponds to the detachment of an individual pillar as can be seen in Figure 2a. In principle the adhesive properties at low preload can be controlled by the number of LP chosen for the sample. With increasing number of LP, the pull-off force and work of adhesion is expected to increase, meeting a natural limit at the values achieved for samples with only one distinct length of pillars.

3.2. Medium Preload

Increasing the compressive preload causes the LP to be compressed in such way that SP also form contact. This sudden increase in contact elements results in two effects. First, the effective stiffness of the sample changes and becomes stiffer. This is reflected in the suddenly increasing slope in the compressive part of the force–displacement curve in Figure 2a. And second, the overall contact area is suddenly increased, leading to a higher pull-off force, which is reflected in the absolute value of the pull-off force, the increase in the tensile part of Figure 2b which corresponds to the work of adhesion, and in the increasing number of detachment events as shown in Figure 2b. While the pull-off force for low preload is expected to be only dependent on the number of LP, the pull-off force at medium preload where LP and SP are in contact depends on both the ratio of LP to SP, on the height difference between SP and LP and on their AR.

3.3. High Preload

If a certain preload range is overcome, the pillars buckle as can be seen in Figure 2c. In earlier studies, the buckling event was closely investigated and it was found that a minimum AR is necessary for buckling as well as that buckling leads to a loss in tip contact which results in almost complete loss in adhesion.[8,14] A similar effect is found here, where the buckling reduces adhesion significantly.

3.4. Analysis of Adhesive Properties

The following equations describe the mechanical response of the adhesive as a function of geometric parameters and of adhesive and mechanical properties. Consider the preload P_p to be below the threshold $P_{p,1}$ where the SP form contact with the probe. The pull-off force P_c is then defined simply by the number of LP, n_{LP}, multiplied with the adhesive force generated by each pillar F_{LP}:

$$P_c = F_{LP} \times n_{LP} \quad \text{For} \quad P_p < P_{p,1} \tag{1}$$

As soon as the critical threshold $P_{p,1}$ is overcome a number of SP, n_{SP}, form contact with the probe and contribute with an additional adhesive force F_{SP} to the overall adhesion. However, the LP need to be compressed to allow the SP to form contact. Thus, elastic energy is stored in the LP which reduces adhesion. The force generated by the stored elastic energy is identical to the force necessary to compress the LP, $F_{compr,LP}$, multiplied by the number of LP, thus:

$$P_c = F_{LP} \times n_{LP} + F_{SP} \times n_{SP} - F_{compr,LP} \times n_{LP} \quad \text{For} \quad P_{p,1} < P_p < P_{p,2} \tag{2}$$

whereas $P_{p,2}$ is the preload at which the structures buckle. Finally, at high preload beyond the buckling preload $P_{p,2}$ the pull-off force drops to the buckling pull-off force $P_{c,buck}$, or:

$$P_c = P_{c,buckling} \times (n_{LP} + n_{SP}) \quad \text{For} \quad P_p > P_{p,2} \tag{3}$$

Thus, by measuring the adhesive force of a single SP and a single LP and extracting the adhesive force and the load necessary for a certain compression may be sufficient to describe the elastic deformation behavior and the adhesive properties of the samples with pillars of different lengths. The adhesive forces F_{LP} and F_{SP} are a function of tip radius r and AR,[15] while the compressive force $F_{compr,LP}$ mainly depends on the AR and the Young's Modulus E.[16] Note that no coupling between the pillars is assumed in this simple model. Also, the collective buckling of pillars with different lengths is difficult to determine.

The results in Figure 3 indicate that both the AR and the measurement velocity influence the adhesive performance. We found that an increase in AR leads to a decrease in adhesion. While the difference between AR 4.0 and AR 4.5 are negligible, the samples with AR 5.0 show a notable lower adhesion. Earlier studies on micropatterned surfaces have reported that a higher AR results in higher adhesion,[17] if the samples are tested with a spherical probe. This can be explained by the reduced effective modulus of the high AR structures, which allows a deeper indentation of the spherical probe into the structures and, thus, resulting in a larger contact area at similar preload. A more recent study using macroscopic pillars and a flat probe revealed that, above a certain AR, no increase of adhesion as a function of AR is found.[15,18] Thus, it is surprising that in the present study adhesion is reduced with increasing AR. A possible explanation for our results is that LP are less stable with respect to bending compared to shorter pillars. This might influence the fabrication of double mushroom tips, especially the second to last step indicated in **Figure 4**. A decreased bending resistance

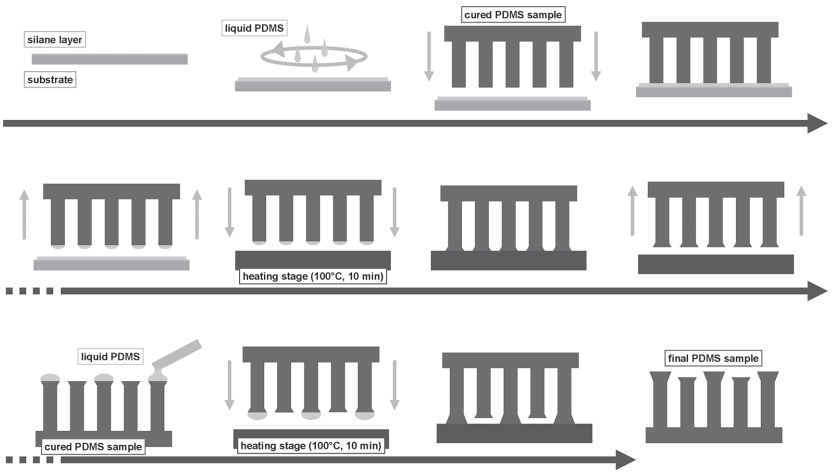

Figure 4. Schematic of mushroom tip preparation. A substrate is silanized and spin coated with liquid PDMS. A previously prepared pillar sample is dipped into the liquid PDMS layer forming droplets on the pillar tips. After pressing the pillars onto a heating stage, mushroom tips are formed. Subsequently, droplets of liquid pillars are applied to selected pillars and the curing process is repeated, resulting in mushroom shaped pillars of different length.

might lead to a slightly tilted mushroom tip which will certainly decrease adhesion.

The results in Figure 3 also show that adhesion depends on the measurement velocity. While for the AR 4.0 structures the pull-off forces are similar for both tested measurement velocities of 20 and 60 μm s^{-1}, tests on AR 4.5 and AR 5.0 samples show that the pull-off force is significantly reduced if tested with the higher velocity. This effect is surprising as it is usually found that adhesion increases with increasing testing velocity due to an increased viscoelastic loss.[19] Following the argument of less stable pillars with increasing AR and a resulting imperfection of the pillar tip alignment during sample preparation for high AR pillars as stated in the previous paragraph, this effect may be explained as follows. With increasing testing velocity, the time to form intimate contact is reduced. PDMS is known to show viscoelastic behavior, especially for loading frequencies between 0.1 and 100 Hz.[20] Thus, increasing testing velocity may deteriorate the conformation of the pillar tip to the probe. This would result in a decrease of adhesion with increasing testing velocity. Indeed, the simpler to fabricate AR4 structures show basically no velocity effect, while the more difficult to fabricate AR4.5 and AR5 pillars show a significant velocity effect. Thus, it is likely that the velocity effect may be caused by the sample preparation.

One final remark has to be given with regard to the scatter of the experimental data. From the data given in Supporting Information it becomes clear that the relatively large error bars in Figure 3 do not origin from poorly defined adhesive properties but are caused by the variation between different samples and/or the tested sample rotation. The switching behavior for single tests is usually much better defined as suggested by Figure 3 and is well represented with the result shown in Figure 2. The reason for the large variety between different samples is most probably due to the manual fabrication method of the double mushroom. Precise positioning of droplets with exactly the same size and preparation of LP with exactly the same length is a process which is almost impossible by manual fabrication. Thus, the adhesive properties at different switching levels will be directly influenced, causing the observed large overall error.

4. Conclusions

In this paper we present a bioinspired switchable adhesive where the adhesive state can be switched by application of compressive preload. The system has—in contrast to other switchable adhesives—three adhesive states, namely low adhesion at low preload, high adhesion at medium preload, and very low adhesion at high preload. To obtain such an adhesive we developed a new fabrication process using two subsequent inking and dipping steps, resulting in samples with pillars of two distinct lengths. By in situ observation we could show that the low adhesive state is caused by attachment of only LP, the high adhesive state by full contact of all pillars, and the very low adhesive state by collective buckling of the pillars. Adhesion experiments with different AR and testing velocity showed that adhesion drops with increasing AR and testing velocity, which may be explained by viscoelastic behavior of the chosen elastomeric material. We also presented a simple model which allows estimation of the different adhesive states based on single pillar measurements.

For future studies, an optimized and automated fabrication method might lead to a higher reproducibility in between different samples. Also, by fabrication of samples having pillars of multiple lengths, more than three adhesive states may be accessible. Such samples could give access up to an almost continuous switching behavior. These new adhesives may find various applications, for example, in transportation, handling, and robotics.

5. Experimental Section

5.1. Sample Fabrication

Templates for molding were prepared by milling of multiple macroscopic pillar assemblies into aluminum as published in earlier studies.[15,16,18] A cavity of 3 mm depth containing hexagonally arranged holes with a diameter of 400 μm were milled. Three different aluminum templates were fabricated which supported a center pillar, six surrounding pillars, and an additional 12 holes surrounding the seven center holes. The holes were 1600, 1800, and 2000 μm deep, resulting in an aspect ratio (AR) of 4.0, 4.5, and 5.0, respectively. The center–center distance of the pillars was 800 μm for all molds. After the milling process, the templates were cleaned with isopropanol and milling residues like metal splinters were removed by several molding steps.

Samples were cast using polydimethylsiloxane (PDMS, Sylgard 184, Dow Corning) in a 10:1 ratio of prepolymer to cross-linker. PDMS is a widely used material system with superior molding properties and easy handling. All samples were prepared by filling the template with the mixed liquid PDMS, degassing in a desiccator until no bubbles were visible and curing in an oven for 2 h at 75 °C.

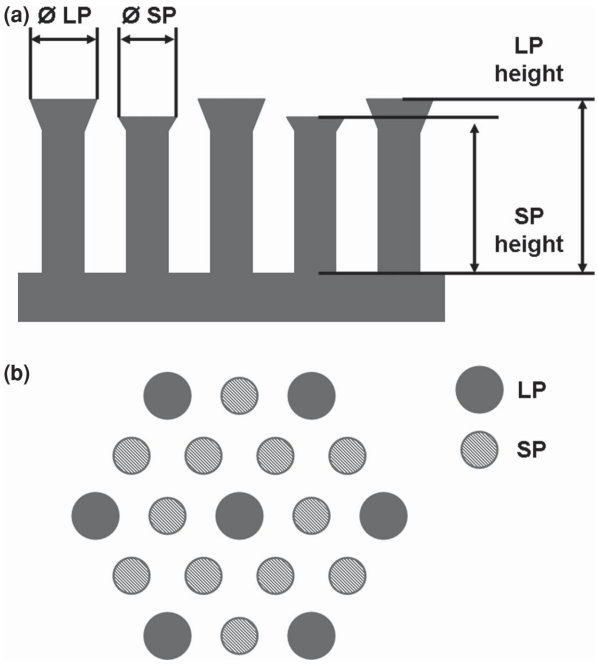

Figure 5. The schematic of a sample indicates SP and LP as well as their respective tip diameters. All geometric parameters were measured using an optical microscope.

5.2. Fabrication of Mushroom Tips

The pillar tips were modified using a custom-made dipping device, which allows quick and reproducible preparation of mushroom shaped tips. The device is composed of a positioning stage and a vacuum sample-holder, which can be aligned by means of two alignment screws. The vacuum holder can be manually moved in z-direction for the dipping process. The initial preparation steps were performed as follows and are schematically described in Figure 4.

i. Prior to molding the substrates were silanized to allow easy removal of PDMS after curing. For vapor deposition of the silane, a vial with 1 µL of Trichloro(1H,1H,2H,2H-perfluorooctyl)silane was placed together with the glass substrates in a desiccator and submitted to vacuum until the silane evaporated completely. The substrates were then placed in an oven at 95 °C for 30 min to stabilize the silane layer.
ii. The prepolymer and the cross-linker of the PDMS kit were mixed in a 10:1 ratio and gas bubbles were removed in a desiccator. Afterwards, 0.5 mL of the degassed PDMS was placed in the middle of a 35 mm substrate and spun at 300 rpm with an acceleration of 5000 rpm s^{-1} for 300 s, resulting in a 0.5 mm thick liquid PDMS layer.
iii. The previously cast pillar samples (Section 2.1) were fixed with the pillars pointing downwards and dipped into the thin PDMS layer, resulting in small droplets of PDMS on the pillar tips.
iv. The samples were then pressed onto a smooth silanized glass substrate and kept at 100 °C for 10 min to achieve the desired tip shape.
v. To achieve samples having pillars of different length, droplets of liquid degassed PDMS were positioned manually on selected pillars using tweezers with a very sharp tip. The selected pillars were the center pillar and the 12 pillars surrounding the seven inner pillars (see also **Figure 5**).
vi. The subsequent process was identical to the previously described one, namely pressing the sample smoothly against a silanized aligned glass substrate, curing at 100 °C for 10 min and final detachment.

The whole dipping process was monitored in situ by an optical camera.

5.3. Adhesion Measurements

Adhesion measurements were performed using the custom-made setup MAD, which is described in ref.[21] In short, the PDMS sample was fixed to a glass slide and placed on a high precision moving and tilting stage. Forces were sensed by measuring the deflection of a metallic cantilever with a spring constant of 2524 N m^{-1} by laser interferometry. The cantilever was equipped with a smooth and aligned glass probe. Measurements were performed by approaching the sample with a defined velocity, applying a predefined (positive) compressive preload, retracting of the sample and obtaining the respective (negative) tensile pull-off force. Testing velocities were chosen to be 20 and 60 µm s^{-1}, respectively. The preload was varied in an adequate range to receive preload dependent pull-off force data. All measurements were monitored using an optical camera. All samples were tested at three different rotation angles (0°, 120°, and 240°) with respect to the vertical axis to minimize effects due to misalignment.[18,21]

Figure 5a shows a schematic of samples with double mushrooms and their geometrical features. In Figure 5b, a top view of the sample is schematically shown to indicate, which positions represent LP and SP. Thus, the samples consist of seven LP and 12 SP.

Supporting Information

Supporting Information is available from the Wiley Online Library or from the author.

Acknowledgements

The authors thank the mechanical workshop for template fabrication and Joachim Blau for help with the adhesion tester. The research leading to these results has received funding from the European Research Council under the European Union's Seventh Framework Program (FP/2007-2013)/ERC Grant Agreement No. 340929.

Received: January 20, 2015
Revised: February 13, 2015
Published online: March 16, 2015

[1] E. Kroner, C. S. Davis, *J. Adhes.* **2015**, *91*, 6, 481.
[2] L. Heepe, S. N. Gorb, *Annu. Rev. Mater. Res.* **2014**, *44*, 173.
[3] a) M. Kamperman, E. Kroner, A. del Campo, R. M. McMeeking, E. Arzt, *Adv. Eng. Mater.* **2010**, *12*, 335; b) D. Sameoto, C. Menon, *Smart Mater. Struct.* **2010**, *19*, 103001.
[4] K. Autumn, N. Gravish, *Philos. Trans. R. Soc. A* **2008**, *366*, 1575.
[5] a) K. Autumn, A. Dittmore, D. Santos, M. Spenko, M. Cutkosky, *J. Exp. Biol.* **2006**, *209*, 3569; b) B. Aksak, M. P. Murphy, M. Sitti, *Langmuir* **2007**, *23*, 3322.
[6] a) K. Autumn, M. Sitti, Y. A. Liang, A. M. Peattie, W. R. Hansen, S. Sponberg, T. Kenny, R. Fearing, J. N. Israelachvili, R. J. Full, *Proc. Natl. Acad. Sci. USA* **2002**, *99*, 12252; b) E. Arzt, S. Gorb, R. Spolenak, *Proc. Natl. Acad. Sci. USA* **2003**, *100*, 10603; c) J. Davies, S. Haq, T. Hawke, J. P. Sargent, *Int. J. Adhes. Adhes.* **2009**, *29*, 380; d) A. Del Campo, C. Greiner, E. Arzt, *Langmuir* **2007**, *23*, 10235; e) A. K. Geim, S. V. Dubonos, I. V. Grigorieva, K. S. Novoselov, A. A. Zhukov, S. Y. Shapoval, *Nat. Mater.* **2003**, *2*, 461; f) S. Gorb, M. Varenberg, A. Peressadko, J. Tuma, *J. R. Soc., Interface* **2007**, *4*, 271; g) C. Greiner, A. del Campo, E. Arzt, *Langmuir* **2007**, *23*, 3495; h) L. Heepe, G. Carbone, E. Pierro, A. E. Kovalev, S. N. Gorb, *Appl. Phys. Lett.* **2014**, *104*; i) L. Heepe, A. E. Kovalev, A. E. Filippov, S. N. Gorb, *Phys. Rev. Lett.* **2013**, *111*, 104301;

j) L. Heepe, M. Varenberg, Y. Itovich, S. N. Gorb, *J. R. Soc., Interface* **2011**, *8*, 585; k) H. E. Jeong, J. K. Lee, H. N. Kim, S. H. Moon, K. Y. Suh, *Proc. Natl. Acad. Sci. USA* **2009**, *106*, 5639; l) K. Jin, Y. Tian, J. S. Erickson, J. Puthoff, K. Autumn, N. S. Pesika, *Langmuir* **2012**, *28*, 5737; m) D. Sameoto, C. Menon, *J. Micromech. Microeng.* **2009**, *19*, 115026; n) D. Sameoto, H. Sharif, C. Menon, *J. Adhes. Sci. Technol.* **2012**, *26*, 2641; o) R. Spolenak, S. Gorb, H. Gao, E. Arzt, *Proc. R. Soc. A* **2005**, *461*, 305; p) M. Varenberg, S. Gorb, *J. R. Soc., Interface* **2008**, *5*, 785; q) B. Yurdumakan, N. R. Raravikar, P. M. Ajayan, A. Dhinojwala, *Chem. Commun.* **2005**, 3799.

[7] M. T. Northen, C. Greiner, E. Arzt, K. L. Turner, *Adv. Mater.* **2008**, *20*, 3905.

[8] D. Paretkar, M. Kamperman, A. S. Schneider, D. Martina, C. Creton, E. Arzt, *Mater. Sci. Eng. C* **2011**, *31*, 1152.

[9] J. Cui, D.-M. Drotlef, I. Larraza, J. P. Fernández-Blázquez, L. F. Boesel, C. Ohm, M. Mezger, R. Zentel, A. del Campo, *Adv. Mater.* **2012**, *24*, 4601.

[10] M. J. Vogel, P. H. Steen, *Proc. Natl. Acad. Sci. USA* **2010**, *107*, 3377.

[11] N. Nadermann, J. Ning, A. Jagota, C. Y. Hui, *Langmuir* **2010**, *26*, 15464.

[12] H. E. Jeong, M. K. Kwak, K. Y. Suh, *Langmuir* **2010**, *26*, 2223.

[13] S. Reddy, E. Arzt, A. del Campo, *Adv. Mater.* **2007**, *19*, 3833.

[14] a) D. R. Paretkar, M. D. Bartlett, R. McMeeking, A. J. Crosby, E. Arzt, *J. Adhes.* **2013**, *89*, 140; b) D. Paretkar, A. S. Schneider, E. Kroner, E. Arzt, *MRS Commun.* **2011**, *1*, 53.

[15] M. Micciché, E. Arzt, E. Kroner, *ACS Appl. Mater. Interfaces* **2014**, *6*, 7076.

[16] E. Kroner, E. Arzt, *J. Mech. Phys. Solids* **2013**, *61*, 1295.

[17] C. Greiner, A. del Campo, E. Arzt, *Langmuir* **2007**, *23*, 3495.

[18] E. Kroner, E. Arzt, *Int. J. Adhes. Adhes.* **2012**, *36*, 32.

[19] a) G. Castellanos, E. Arzt, M. Kamperman, *Langmuir* **2011**, *27*, 7752; b) S. Vajpayee, R. Long, L. Shen, A. Jagota, C.-Y. Hui, *Langmuir* **2009**, *25*, 2765.

[20] I.-K. Lin, K.-S. Ou, Y.-M. Liao, Yan Liu, K.-S. Chen, X. Zhang, *J. Microelectromech. Syst.* **2009**, *18*, 1087.

[21] E. Kroner, J. Blau, E. Arzt, *Rev. Sci. Instrum.* **2012**, *83*, 016101.